Femtosecond time-domain observation of atmospheric absorption in the near-infrared spectrum

T. J. Hammond, Sylvain Monchocé, Chunmei Zhang, Graham G. Brown, P. B. Corkum, and D. M. Villeneuve

Femtosecond Time-Domain Observation of Atmospheric Absorption in the Near Infrared

T. J. Hammond,[1, 2] Sylvain Monchocé,[1] Chunmei Zhang,[1] Graham G. Brown,[1] P. B. Corkum,[1] and D. M. Villeneuve[1]

[1] *Joint Attosecond Science Laboratory, National Research Council of Canada and University of Ottawa,*
100 Sussex Drive, Ottawa, ON K1A 0R6, Canada
[2] *University of Central Florida, 4304 Scorpius St, Orlando, FL 32816, United States*
(Dated: November 15, 2016)

As light propagates through a medium, absorption caused by electronic or rovibrational transitions is evident in the transmitted spectrum. The incident electromagnetic field polarizes the medium and the absorption is due to the imaginary part of the linear susceptibility. In the time domain, the field establishes a coherence in the medium which radiates out of phase with the initial field. This coherence can persist for tens of picoseconds in atmospheric molecules such as H_2O. We propagate a few-cycle laser pulse centered at 1.8 μm through the atmosphere and measure the long-lasting molecular coherence in the time domain by high-order harmonic cross-correlation. The measured optical free induction decay of the pulse is compared with a calculation based on the calculated rovibrational spectrum of H_2O absorption.

PACS numbers: May be entered using the \pacs{#1} command.

I. INTRODUCTION

Coherent table-top sources with energies greater than 300 eV [1–3] − the so-called 'water window' − and solid state spectroscopy [4, 5] motivate the next generation of lasers for high harmonic generation (HHG) experiments. Both cases benefit from high power, mid-infrared (IR), ultrashort driving fields. In the former case, the ponderomotive energy, which scales with λ^2, where λ is the driving field wavelength, determines the generated bandwidth to create a coherent source in the soft X-ray region with attosecond temporal resolution [6, 7]. In the latter case, the small semiconductor bandgap decreases the threshold for optically induced damage; the lower photon energy from longer wavelength sources mitigates this damage [8]. In both cases, a shorter pulse duration leads to more efficient harmonic generation and lower ionization. These short pulses require precise phase control over a large spectral bandwidth [9–11]. However, several small molecules abundant in air strongly absorb in the mid-IR, including H_2O and CO_2 [12]. In particular, water has several absorption bands throughout the IR, each consisting of many rovibrational transitions.

Absorption leads to the attenuation of the field as it propagates through a medium. Absorption of a certain wavelength of light by a molecular transition seems straightforward: the absorption line (corresponding to the molecular transition) imprints on the spectrum that transmits through the absorbing medium. The picture is actually more complicated than it first seems, particularly for broad bandwidth pulses that have pulse durations much shorter than the molecular transition decay time. Consider a laser pulse propagating through a medium composed of a simple two-level "molecule". The broad bandwidth of the short pulse will cause some excitation to the upper level that will induce an oscillating dipole moment in the molecule, radiating at the frequency of the transition. This radiation will decrease exponentially until the molecule has radiated away all of its absorbed energy [13]. The induced polarization is out of phase with the laser pulse, and the destructive interference will cause a hole in the transmitted spectrum.

The long decaying emission is well known in nuclear magnetic resonance, where it is called free induction decay. A pioneering experiment by Brewer and Shoemaker [14] used a CW laser and a pulsed DC electric field to Stark-shift the resonance, and observed the beat frequency of the shifted emission, measuring optical free induction decay. Transients have been measured by linear autocorrelation [15], but this is effectively a spectral measurement by Fourier transform spectroscopy. Lozovoy *et al.* [16] observed time-gated free induction decay from iodine vapor. Dual frequency combs can measure the free induction decay over several nanoseconds, where the minimal temporal resolution is determined by two laser spectral bandwidths [17].

It seems remarkable that a femtosecond pulse propagating through an absorbing medium creates a coherent ensemble of oscillating dipoles in its wake, trailing the pulse by many picoseconds, and that the emission from these dipoles radiates in the forward direction in a phase-matched manner. It is increasingly important to understand the re-emission process. For example, attosecond transient absorption experiments [18] show that, by modifying the energy levels of the emitting atoms *after* the attosecond pulse (much like Brewer and Shoemaker [14]), the absorption line shape can be changed between Lorentzian and Fano.

Femtosecond time-domain measurements typically require a nonlinear medium in which to mix the frequency components of the two inputs to obtain a cross-correlation signal at a new frequency. For example, sum frequency mixing of two pulses in a nonlinear crystal generates a third frequency at the sum of the other two frequencies. To perform the time-domain measurement, one input is delayed in time relative to the other. The nonlin-
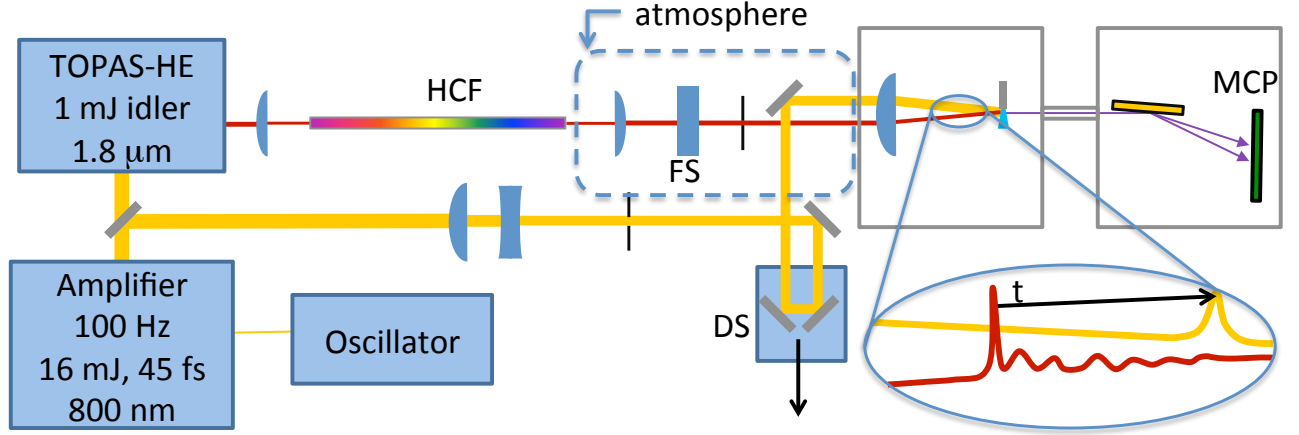
FIG. 1. Experimental setup. The OPA idler spectrum centered at 1.8μm is broadened in the hollow core fiber (HCF), and compressed with 3 mm fused silica (FS). The delay stage (DS) controls the time delay of the two arms. The two beams are focussed into the gas jet in a vacuum chamber, and the XUV light is passed through a differential pumping tube to a detection chamber, containing a grazing angle diffraction grating and MCP.

ear mixing process creates frequency sidebands that can be filtered, either in frequency or in space, to give the cross-correlation signal versus time.

To measure the optical free induction decay, we use high-order harmonic generation (HHG) cross-correlation. HHG is a three step process [19]. The first step, ionization, requires a very strong driving field to separate an electron from an atom or molecule, typically an intensity on the order of 10^{14} W/cm^2. In the second step, the driving field accelerates the freed electron. In the third step, the recombination of the electron with the parent ion releases a burst of radiation in the extreme ultraviolet, coherent with the driving field. This event occurs twice per optical cycle; the periodicity of the driving field yields a series of odd harmonics. Perturbing the periodicity leads to sidebands in the harmonic spectrum.

Because the perturbation acts mainly on the free electron, the electron trajectory is surprisingly sensitive to the perturbing field and shows strong signatures in the harmonic spectrum from relatively weak perturbations [20, 21]. Here we will use high harmonic generation (HHG) to perform a time-domain cross correlation of the free induction decay. The emitted frequencies are given by integer combinations of the two optical frequencies, $\Omega = n_{800}\omega_{800} + n_{1800}\omega_{1800}$, where $n_{800} + n_{1800}$ is odd. If the second field is weak, then it contributes only one photon, i.e. $n_{1800} = 1$ and n_{800} is even, and the intensity of the new frequencies scales linearly with the intensity of the second field [22].

II. EXPERIMENTAL SETUP

The setup is shown in Fig. 1. We use a Ti:Sapphire (Ti:S) amplifier, total output energy of 16 mJ and 45 fs pulse duration, and a beamsplitter splits the beam into two arms. We direct one arm to an optical parametric amplifier (OPA TOPAS-HE). We couple the idler output of the OPA into a hollow-core fiber, 500 μm diameter, differentially pumped with 1 Bar argon to broaden the spectrum [23]. We use approximately 3 mm of fused silica to compress the pulse to near transform limited pulse duration of 12 fs with 450 μJ energy centered at 1.8 μm [24]. For the experiment, we reduce the energy with an iris to 350 μJ. A 2:1 telescope decreases the far field beam size of the other arm, and a computer controlled delay stage adjusts the relative timing of the two arms.

The beams are non-collinearly focussed (f = 300 mm, angle of separation 20 mrad) into a gas jet (backing pressure 4 Bar). Each beam has sufficient intensity to generate high harmonics in the gas jet. An extreme ultraviolet (XUV) spectrometer with micro-channel plate (MCP) gives us spatio-spectral information on the high harmonics generated by the two arms. The spectra generated from the 800 nm and the OPA sources are vertically separated on the MCP, allowing us to monitor the intensity of each beam during the time delay scan. When the two pulses are overlapped in time, new combination frequencies are present. These new frequencies are the cross correlation signal, which provides a measurement of the time profile of the 1.8 μm pulse envelope.

III. EXPERIMENTAL RESULTS

The spectrogram is shown in Fig. 2. The strong vertical lines are harmonics generated from the strong 800 nm arm. The cutoff harmonic near 42 eV (27th harmonic) implies the peak intensity is 1.3×10^{14} W/cm^2. The harmonics are normalised to the sum of harmonics 19, 21, and 23 (this is necessary when discussing the influence of the perturbation amplitude, below). At time zero, the
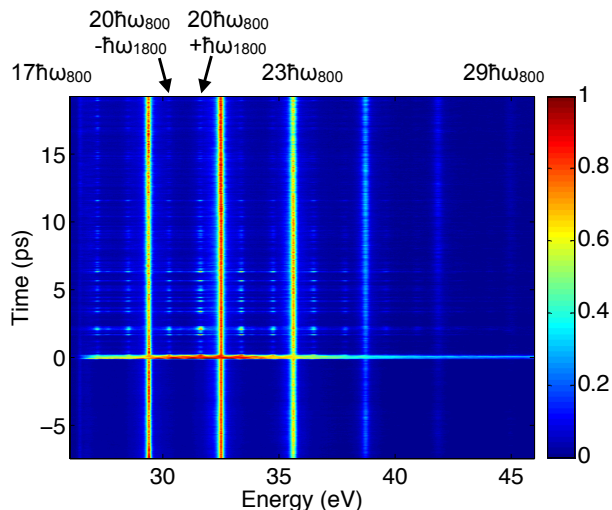
FIG. 2. Delay dependence of the high harmonic signal, H17 H29 of 800nm. At time zero the 1.8 μm and 800 nm beams overlap, leading to a spectral continuum. For $t < 0$, the 800 nm pulse arrives before the 1.8 μm pulse. For $t > 0$, the 1.8 μm pulse arrives first. When $t > 0$, the tail in the 1.8 μm pulse leads to spectral sidebands between the 800 nm harmonic orders, providing the cross correlation signal.

few cycle idler of the OPA is overlapped spatially and temporally with the 800 nm arm. As expected, there is a broad, nearly continuous spectrum extending to above 80 eV (the edge of the MCP, not shown). When the 800 nm pulse arrives first (t<0), the spectrum shows no sidebands. However, when the OPA arrives first (t>0), sidebands appear between the 800 nm harmonic orders due to wave mixing of the two frequencies. A temporal modulation in the sidebands is evident, and was repeatable from day to day.

The spacing of the odd harmonics of the 800 nm arm is measured to be 2×1.55 eV. The spacing of the odd harmonics from the OPA alone (not shown) is 2×0.73 eV, implying a central wavelength of 1.70 μm. The frequency of the sidebands is given by $\Omega = n_{800}\omega_{800} \pm \omega_{1800}$ where n_{800} is an even integer. The sideband positions show that $\omega_{1800} = 0.66$ eV, which is different from the central frequency of the 1.8 μm pulse of 0.73 eV. This shows that the optical free induction decay has a wavelength around 1.85 μm, corresponding to the absorption band of H_2O.

IV. MODEL

The intensity of the sidebands is dependent on the intensity of both the driving field and the perturbation. We calculate the sensitivity of HHG to the perturbation using the strong field approximation (SFA) [25], with the ionization rates based on Ref. [26]. For the simulation, the driving field intensity is 1.3×10^{14} W/cm^2, with a 10 cycle full width at half maximum pulse duration, while the perturbation pulse envelope is constant.
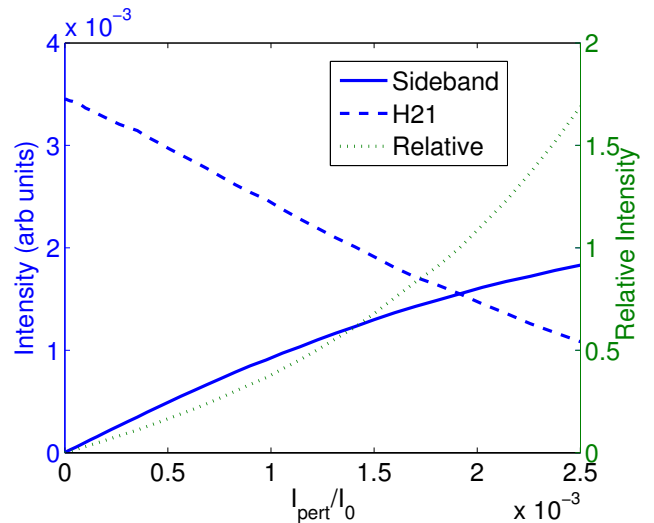

FIG. 3. Calculated sideband intensity (solid blue line) relative to H21 (dashed blue) as a function of the perturbing intensity. The strong 800 nm pulse has a peak intensity of $I_0 = 1.3 \times 10^{14}$ W/cm^2. The relative sideband intensity (green dotted) scales almost linearly with the intensity I_{pert} of the 1.8 μm perturbing pulse for low intensities.

The sideband intensity as a function of the relative intensity of the perturbation to the driving field is shown in Fig. 3. The sideband intensity scales almost linearly with the intensity of the perturbing pulse, consistent with previous experiments [22]. We find that the sensitivity of the HHG process to a perturbation – the relative sideband intensity as a function of the relative perturbation intensity – is not strongly dependent on the wavelengths of the driving field or the perturbation. Thus the sideband intensity provides an almost-linear cross correlation measurement of the intensity of the 1.8 μm pulse tail.

To compare with the measured free induction decay of the 1.8 μm pulse with theory, we take the absorption coefficients from the High Resolution Transmission (HITRAN) database [27]. The parameters used were for the USA model at mid latitude, summer air conditions (conditions in the lab were approximately 23°C with 30% humidity). This model includes rovibrational transitions mostly corresponding to $\nu_1 + \nu_2$ and $\nu_2 + \nu_3$ overtones of the vibrational modes in the Ω band of H_2O. From the absorption coefficients, $\alpha(\omega)$, we are able to calculate the index of refraction, $n(\omega)$, using the Kramers-Kronig relations [28]. Shown in Fig. 4(a) is the absorption spectrum of air using HITRAN and the calculated index of refraction spectrum.

We calculate the effect of propagation through $L = 7$ m of air on a simulated $\Delta t = 12$ fs full width at half maximum (FWHM) Gaussian envelope duration pulse centered at $\lambda_1 = 1.8\mu$m. That is,

$$E_0(t) = E_0 \exp\left(-\frac{t^2}{2\tau^2}\right)e^{-i\omega_1 t}, \qquad (1)$$
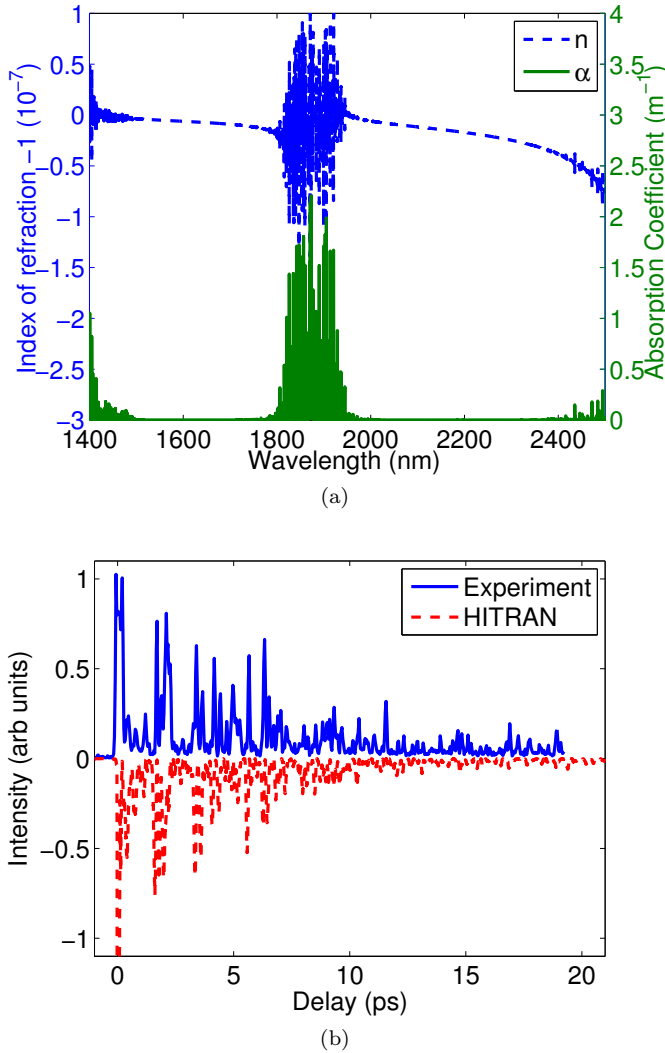
(a)

(b)

FIG. 4. (a) Calculation of the absorption coefficient of air (green solid line) in the near-IR using the HITRAN model. Also shown is the calculated index of refraction (blue dash). (b) Measured intensity profile of the free induction decay signal following the 1.8 μm pulse after propagation through the laboratory air (blue solid). Also shown (inverted, red dash) is the calculated decay of a 12 fs (Gaussian) 1.8 μm pulse propagating through 7 m of air using the HITRAN absorption.

where $\Delta t = 2\tau\sqrt{ln(2)}$ and $\omega_1 = 2\pi c/\lambda_1$. The spectrum is then

$$E_0(\omega) = \tau E_0 \exp\left[-(\omega - \omega_1)^2 \frac{\tau^2}{2}\right]. \qquad (2)$$

The total phase imparted on the propagating pulse is $\phi(\omega) = \frac{\omega}{c}n(\omega)L + i\frac{\alpha(\omega)}{2}L$. The real and imaginary parts of the spectral transmission in Fig. 4(a), multiplied by the spectrum of the pulse, are Fourier-transformed into the time domain. That is

$$|E(t)|^2 \propto |\mathcal{F}\{E_0(\omega)e^{i\phi(\omega)}\}|^2. \qquad (3)$$

The intensity of the calculated tail takes into account the relative peak intensity of the 800 nm and 1.8 μm beams and the sideband intensity scaling calculated in Fig. 3, determining the proportionality constant. The resulting tail is shown in Fig. 4(b), along with the experimental sideband trace at 31.64 eV. Using only the absorption spectrum also leads to a tail, however the amplitude differs by a factor of two and there is no causality. The data are normalized to the maximum harmonic intensity, H21 in Fig. 2. The calculated tail intensity agrees well with the measured sideband intensity. From the agreement of the simulated tail with the measurement sidebands of the high harmonics, we see that the coherence of the free induction decay stimulated by the few cycle laser pulse lasts over 20 ps. We can also see from Fig. 4(a) why the harmonics of the OPA pulse give a central wavelength of 1.7 μm, but the free induction decay re-emission has a central wavelength of 1.85 μm.

V. CONCLUSIONS

The optical free induction decay measured via HHG cross-correlation demonstrates that the coherence induced on a few cycle pulse due to atmospheric H_2O absorption in the near-IR is maintained for tens of ps. The absorption of water in the near- and mid-IR has important consequences for next generation HHG sources [29, 30]. The absorption bands cause reshaping of the ultrashort driving field in the time domain. For few cycle pulses, this leads to decreased peak intensity, while the long tail resulting from the coherent free induction decay leads to complications in femtosecond and attosecond pump-probe experiments.

VI. ACKNOWLEDGEMENTS

[1] M.-C. Chen, P. Arpin, T. Popmintchev, M. Gerrity, B. Zhang, M. Seaberg, D. Popmintchev, M. M. Murnane, and H. C. Kapteyn, Physical Review Letters **105**, 173901 (2010).

[2] N. Ishii, K. Kaneshima, K. Kitano, T. Kanai, S. Watanabe, and J. Itatani, Nature Communications **5**, 3331

(2014).

[3] F. Silva, S. M. Teichmann, S. L. Cousin, M. Hemmer, and J. Biegert, Nature Communications **6**, 6611 (2015).

[4] O. Schubert, M. Hohenleutner, F. Langer, B. Urbanek, C. Lange, U. Huttner, D. Golde, T. Meier, M. Kira, S. W. Koch, and R. Huber, Nature Photonics **8**, 119 (2014).

[5] G. Vampa, T. J. Hammond, N. Thiré, B. E. Schmidt, F. Légaré, C. R. McDonald, T. Brabec, and P. B. Corkum, Nature **522**, 462 (2015).

[6] T. Popmintchev, M.-C. Chen, D. Popmintchev, P. Arpin, S. Brown, S. Ališauskas, T. Andriukaitis, Giedrius Balčiunas, O. D. Mucke, A. Pugzlys, A. Baltuška, B. Shim, A. Schrauth, Samuel E. Gaeta, C. Hernández-García, L. Plaja, A. Becker, A. Jaron-Becker, M. M. Murnane, and H. C. Kapteyn, Science **336**, 1287 (2012).

[7] Z. Chang, P. B. Corkum, and S. R. Leone, Journal of the Optical Society of America B **33**, 1081 (2016).

[8] S. Ghimire, A. D. DiChiara, E. Sistrunk, P. Agostini, L. F. DiMauro, and D. A. Reis, Nature Physics **7**, 138 (2011).

[9] B. E. Schmidt, A. D. Shiner, M. Giguère, P. Lassonde, C. A. Trallero-Herrero, J.-C. Kieffer, P. B. Corkum, D. M. Villeneuve, and F. Légaré, Journal of Physics B: Atomic Molecular and Optical Physics **45**, 074008 (2012).

[10] T. T. Luu, M. Garg, S. Y. Kruchinin, A. Moulet, M. T. Hassan, and E. Goulielmakis, Nature **521**, 498 (2015).

[11] H. Fattahi, H. G. Barros, M. Gorjan, T. Nubbemeyer, B. Alsaif, C. Y. Teisset, M. Schultze, S. Prinz, M. Haefner, M. Ueffing, A. Alismail, L. Vámos, A. Schwarz, O. Pronin, J. Brons, X. T. Geng, G. Arisholm, M. Ciappina, V. S. Yakovlev, D.-E. Kim, A. M. Azzeer, N. Karpowicz, D. Sutter, Z. Major, T. Metzger, and F. Krausz, Optica **1**, 45 (2014).

[12] A. A. Lanin, A. A. Voronin, A. B. Fedotov, and A. M. Zheltikov, Scientific Reports **4**, 6670 (2014).

[13] R. P. Feynman, R. B. Leighton, and M. Sands, "The feynman lectures on physics," (California Institute of Technology, 1975) Chap. 32.

[14] R. G. Brewer and R. L. Shoemaker, Phys. Rev. A **6**, 2001 (1972).

[15] N. Tsurumachi, T. Fuji, S. Kawato, T. Hattori, and H. Nakatsuka, Optics Letters **19**, 1867 (1994).

[16] V. V. Lozovoy, I. Pastirk, M. G. Comstock, and M. Dantus, Chemical Physics **266**, 205 (2001).

[17] I. Coddington, W. C. Swann, and N. R. Newbury, Opt. Lett. **35**, 1395 (2010).

[18] C. Ott, A. Kaldun, P. Raith, K. Meyer, M. Laux, J. Evers, C. H. Keitel, C. H. Greene, and T. Pfeifer, Science **340**, 716 (2013).

[19] P. B. Corkum, Phys. Rev. Lett. **71**, 1994 (1993).

[20] N. Dudovich, O. Smirnova, J. Levesque, Y. Mairesse, M. Y. Ivanov, D. M. Villeneuve, and P. B. Corkum, Nature Physics **2**, 781 (2006).

[21] H. C. Bandulet, D. Comtois, E. Bisson, A. Fleischer, H. Pépin, J. C. Kieffer, P. B. Corkum, and D. M. Villeneuve, Physical Review A **81**, 013803 (2010).

[22] J. B. Bertrand, H. J. Wörner, H.-C. Bandulet, É. Bisson, M. Spanner, J.-C. Kieffer, D. M. Villeneuve, and P. B. Corkum, Phys. Rev. Lett. **106**, 023001 (2011).

[23] P. Béjot, B. E. Schmidt, J. Kasparian, J.-P. Wolf, and F. Légaré, Phys. Rev. A **81**, 063828 (2010).

[24] B. E. Schmidt, P. Bèjot, M. Giguère, A. D. Shiner, C. Trallero-Herrero, E. Bisson, J. Kasparian, J. P. Wolf, D. M. Villeneuve, J. C. Kieffer, P. B. Corkum, and F. Légaré, Applied Physics Letters **96**, 121109 (2010).

[25] M. Lewenstein, P. Balcou, M. Y. Ivanov, A. L'Huillier, and P. B. Corkum, Phys. Rev. A **49**, 2117 (1994).

[26] G. L. Yudin and M. Y. Ivanov, Phys. Rev. A **64**, 013409 (2001).

[27] L. S. Rothman, I. E. Gordon, Y. Babikov, A. Barbe, D. Chris Benner, P. F. Bernath, M. Birk, L. Bizzocchi, V. Boudon, L. R. Brown, A. Campargue, K. Chance, E. A. Cohen, L. H. Coudert, V. M. Devi, B. J. Drouin, A. Fayt, J. M. Flaud, R. R. Gamache, J. J. Harrison, J. M. Hartmann, C. Hill, J. T. Hodges, D. Jacquemart, A. Jolly, J. Lamouroux, R. J. Le Roy, G. Li, D. A. Long, O. M. Lyulin, C. J. Mackie, S. T. Massie, S. Mikhailenko, H. S. P. Müller, O. V. Naumenko, A. V. Nikitin, J. Orphal, V. Perevalov, A. Perrin, E. R. Polovtseva, C. Richard, M. A. H. Smith, E. Starikova, K. Sung, S. Tashkun, J. Tennyson, G. C. Toon, V. G. Tyuterev, and G. Wagner, Journal of Quantitative Spectroscopy and Radiative Transfer **130**, 4 (2013).

[28] J. D. Jackson, *Classical Electrodynamics* (John Wiley & Sons, Inc, 1999).

[29] M. Gebhardt, C. Gaida, F. Stutzki, S. Hädrich, C. Jauregui, J. Limpert, and A. Tünnermann, Optics Express **23**, 13776 (2015).

[30] S. Duval, M. Bernier, V. Fortin, J. Genest, M. Piche, and R. Vallee, Optica **2**, 623 (2015).